INORGANIC CHEMISTRY
FRONTIERS

RESEARCH ARTICLE

Enhanced relaxivity of Gd^{III}-complexes with HP-DO3A-like ligands upon the activation of the intramolecular catalysis of the prototropic exchange†

Cite this: DOI: 10.1039/d0qi01333a

Luciano Lattuada,*[a] Dávid Horváth,[b] Sonia Colombo Serra,[c] Alberto Fringuello Mingo,[c] Paolo Minazzi,[d] Attila Bényei,[b] Attila Forgacs,[e] Franco Fedeli,[d] Eliana Gianolio,[f] Silvio Aime,[f] Giovanni B. Giovenzana[d,g] and Zsolt Baranyai*[c]

Received 9th November 2020,
Accepted 7th January 2021

DOI: 10.1039/d0qi01333a

rsc.li/frontiers-inorganic

Gadolinium(III) complexes have been employed for more than 30 years as contrast agents in magnetic resonance imaging (MRI). In order to further improve the diagnostic accuracy of enhanced magnetic resonance images or to provide comparable enhancement at a reduced administered dose, current research is focusing on the development of Gd^{III}-complexes characterized by higher relaxivity. In this study we describe the synthesis and the equilibrium, kinetic, relaxation and structural properties of two new Gd^{III}-complexes based on modified 10-(2-hydroxypropyl)-1,4,7,10-tetraazacyclododecane-1,4,7-triacetic acid (HP-DO3A) structure which, due to an intramolecular prototropic exchange, display more than two-fold higher relaxivity compared to currently available Gd^{III}-based MRI contrast agents.

Introduction

Magnetic Resonance Imaging (MRI) is one of the most powerful *in vivo* diagnostic techniques currently employed in clinical practice. Acquired MR images are essentially proton signal intensity maps that reflect the distribution of water molecules within the investigated anatomical regions.[1] MRI has several advantages over other imaging techniques such as computed tomography (CT), ultrasounds (US), single-photon emission computed tomography (SPECT) and positron emission tomography (PET). Among these advantages are high spatial resolution and temporal resolution, absence of ionizing radiation, deep tissue penetration and the possibility to acquire three dimensional (3D) anatomical images. Moreover, the administration of an exogenous contrast agent permits the addition of functional information to the already superb anatomical information available, enabling more accurate diagnoses to be made.[2] The contrast agents currently available on the market are based primarily on the paramagnetic ion gadolinium (Gd^{III}).[3] Although other paramagnetic metal ions such as manganese (Mn^{II}) and iron (Fe^{III}) have been utilized in contrast-enhanced MRI procedures, Gd^{III} is the preferred paramagnetic ion because its seven unpaired electrons and long electronic relaxation time present optimal relaxometric properties.[4] In gadolinium-based contrast agents (GBCAs) Gd^{III}-ion is coordinated with acyclic or cyclic polyaminopolycarboxylic chelating agents such as diethylenetriaminepentaacetic acid (DTPA)[5] or 1,4,7,10-tetraazacyclododecane-1,4,7,10-tetraacetic acid (DOTA) to render them safe for *in vivo* administration.[6]

The efficacy of a GBCA is determined by its relaxivity, which is a measure of the agent's ability to shorten the relaxation time of water protons in its immediate environment. All the commercial GBCAs have one coordinated water molecule (q = 1) and their longitudinal r_1 relaxivity values in plasma range between approximately 3.6 and 7.9 mM^{-1} s^{-1} at 1.5 T and 37 °C.[7] GBCAs have been used in more than a third of all MRI procedures for more than three decades and have an excellent safety profile in terms of immediate adverse events.[8]

[a]Innovation Hub, Bracco SpA, Via Caduti di Marcinelle 13, 20134 Milano, Italy. E-mail: luciano.lattuada@bracco.com
[b]Department of Physical Chemistry, University of Debrecen, H-4010 Debrecen, Egyetem tér 1., Hungary
[c]Bracco Research Center, , Bracco Imaging SpAVia Ribes 5, 10010 Colleretto, Giacosa (TO), Italy. E-mail: zsolt.baranyai@bracco.com
[d]CAGE Chemicals, Via Bovio 6, 28100 Novara, Italy
[e]MTA-DE Redox and Homogeneous Catalytic Reaction Mechanisms Research Group, Egyetem tér 1, Debrecen, H-4032, Hungary
[f]Department of Molecular Biotechnologies and Health Science, University of Turin, Via Nizza 52, 10125 Turin, Italy
[g]Dipartimento di Scienze del Farmaco, Università del Piemonte Orientale, Largo Donegani 2/3, Novara, Italy

†Electronic supplementary information (ESI) available. CCDC 2042633. For ESI and crystallographic data in CIF or other electronic format see DOI: 10.1039/d0qi01333a

Unfortunately, certain GBCAs have been associated with an extremely debilitating, often fatal, disease called nephrogenic systemic fibrosis (NSF) in patients with pre-existing severe renal problems[8c] More recently, an additional source of concern has come from the discovery that gadolinium is retained in the brain and body tissues of patients into whom GBCAs are injected.[9] Although no clinical signs or adverse clinical symptoms other than NSF have yet been associated with retained Gd, the phenomenon has been observed to a greater or lesser extent with all GBCAs, even after just a single administration.[9c]

Because GBCAs are indispensable for current MRI procedures, there is renewed focus on the design of agents with enhanced relaxivity which can be used at lower doses than those GBCAs currently approved for clinical use. An example of a newer GBCA is gadopiclenol,[10] a novel macrocyclic GBCA based on the 3,6,9,15-tetraazabicyclo[9.3.1]pentadeca-1(15),11,13-triene-3,6,9-triacetic acid (PCTA) chelating structure.[11] Unlike currently available GBCAs, gadopiclenol coordinates two water molecules (q = 2) and has an r_1 relaxivity of 12.8 mM^{-1} s^{-1} at 1.41 T in human serum at 37 °C.[10]

In looking to develop new higher relaxivity GBCAs, rather than designing and synthesizing new coordinating chelates, we chose to explore the possibility to modify the substituent on the hydroxypropyl arm of an existing GBCA (Gd(HP-DO3A), gadoteridol). Gd(HP-DO3A) is known to have high *in vivo* stability and low toxicity.[12] To this end, we designed two new HP-DO3A derivatives ($\mathbf{L_1}$ and $\mathbf{L_2}$, Scheme 1) characterized by the following features: (1) a macrocyclic HP-DO3A chelating structure to ensure good *in vivo* stability; (2) the presence of a benzyl residue to enable non-covalent binding to biological macromolecules; (3) a network of functional groups able to accelerate the prototropic exchange involving the hydroxyl group of HP-DO3A.

Increased relaxivity of a GBCAs bearing an aromatic ring is a well-known phenomenon.[13] A good example is gadobenate dimeglumine (MultiHance)[14] which shows remarkably higher r_1 relaxivity in plasma compared to water due to interaction of the benzyloxymethyl side-chain with albumin.[15] The intramolecular catalysis of the proton exchange of the coordinated hydroxyl group of Gd(HP-DO3A) still remains a task of considerable importance to attain GBCAs with enhanced relaxivity.[16] Herein we report the synthesis of HP-DO3A derivatives $\mathbf{L_1}$ and $\mathbf{L_2}$, together with the thermodynamic, kinetic, relaxation and structural features of novel Gd$\mathbf{L_1}$ and Gd$\mathbf{L_2}$ complexes.

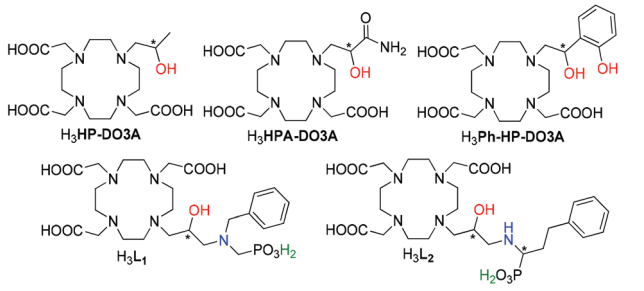

Scheme 1 Structures of the ligands $H_3\mathbf{L_1}$, $H_3\mathbf{L_2}$, H_3**HP-DO3A**, H_3**HPA-DO3A** and H_3**Ph-HP-DO3A**. (*) shows the stereogenic centers.

Results and discussion

Synthesis

To modify the hydroxypropyl chain of the HP-DO3A ligand, we identified the bifunctional chelating agent (BFCA)[17] **1** as a versatile key intermediate, owing to the presence of the reactive primary amine. The synthesis of gadolinium complex Gd$\mathbf{L_1}$ was achieved in four steps (Scheme 2). Compound **1** was prepared according to a literature procedure[18] and *N*-benzylated by reaction with benzaldehyde; the intermediate imine, not isolated, was directly reduced with sodium borohydride to the secondary amine **2**. Reaction of the latter with paraformaldehyde and tri-*t*-butyl phosphite[19] at 70 °C for 6 h leads to the phosphonate *t*-butyl ester **3**, which is then finally and exhaustively deprotected by treatment with trifluoroacetic acid. The chelating agent $\mathbf{L_1}$ was then reacted with $GdCl_3$ in aqueous solution to give the desired complex Gd$\mathbf{L_1}$.

Gd$\mathbf{L_2}$ was synthesized by reacting compound **1** with 3-phenylpropionaldeyde and diethylphosphite at 80 °C for 8 h to give the phosphonate ester **4**. This was then deprotected by sequential treatment with bromotrimethylsilane and trifluoroacetic acid. Final complexation of the chelating agent $\mathbf{L_2}$ with equimolar $GdCl_3$ gave complex Gd$\mathbf{L_2}$. Both complexes were desalted and purified by adsorption and elution on a polystyrene type resin.

Thermodynamic properties of Gd$\mathbf{L_1}$ and Gd$\mathbf{L_2}$ complexes

The Gd^{III}-complexes used as contrast agents in MRI investigations must have high thermodynamic stability to prevent the transmetallation or transchelation reactions with the endogeneous metal ions (*e.g.* Zn^{II}, Cu^{II}, Ca^{II} and Fe^{III}) and chelating

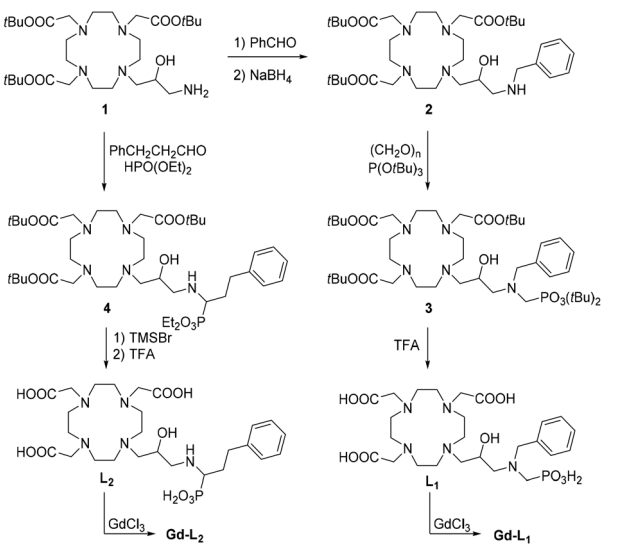

Scheme 2 Synthesis of gadolinium complexes Gd$\mathbf{L_1}$ and Gd$\mathbf{L_2}$.

compounds (*e.g.*: phosphate, carbonate, lactate, amino acids, proteins, *etc.*).[20] In addition, knowledge of the equilibrium properties that characterize the protonation/deprotonation of the Gd^{III} complexes formed with HP-DO3A derivatives is crucial to understand the intramolecular proton exchange processes.[16] The stability and protonation constants of the Ca^{II}-, Zn^{II}-, Cu^{II}- and Gd^{III}-complexes of $\mathbf{L_1}$ and $\mathbf{L_2}$ ligands were determined by pH-potentiometry, ^{1}H NMR relaxometry (Fig. S3†) and spectrophotometry (Fig. S4†). To calculate the stability constants, the protonation constants of the $\mathbf{L_1}$ and $\mathbf{L_2}$ ligands (Table S1†) obtained by pH-potentiometry and NMR spectroscopy (Fig. S1 and S2†) were used. The $\log K_{ML}$ values are summarized and compared with those of the corresponding metal complexes formed by **HP-DO3A** and **HPA-DO3A** in Table 1 and Table S3.† The experimental details, as well as the definitions and equations used to obtain the equilibrium data, are summarized in ESI.†

The $\log K_{ML}$ values of the Gd^{III}-, Ca^{II}-, Zn^{II}- and Cu^{II}-$\mathbf{L_{1,2}}$ complexes (Table 1) are about 2–4 $\log K$ unit smaller than those of the corresponding **HP-DO3A** complexes but very similar to those of the **HPA-DO3A** complexes (Scheme 1). To approach the physiological conditions, we adjusted the ionic strength to 0.15 M with NaCl. It is well known that the protonation constants of ligands in 0.15 M NaCl solution are lower than those determined in 0.1 M KCl or 0.1 M Me_4NCl solutions. The largest difference between the $\log K_i^H$ values obtained in NaCl and KCl or Me_4NCl solutions has been determined for macrocyclic ligands which form relatively stable complexes with Na^+ ion ($\log K_{Na(\mathbf{DOTA})} = 4.38$).[22] Consequently, the equilibrium constants of the metal-complexes formed with $\mathbf{L_{1,2}}$ in 0.15 M NaCl solution are presumably smaller than they would be in 0.1 M KCl, or Me_4NCl. Similar $\log K_{GdL}$ values for Gd$\mathbf{L_{1,2}}$ and Gd(**HPA-DO3A**) obtained at 25° in 0.15 M NaCl solution might be explained by the comparable but minor role of the coordinated alcoholic –OH group in the Gd^{III} – ligand interaction. Interestingly, the $\log K_{MHiL}$ values of Gd$\mathbf{L_{1,2}}$ complexes characterize the protonation of the remote basic phoshonate $-O^-$ and the amino N donor atoms are smaller than those of the free $\mathbf{L_{1,2}}$, which might be explained by the electrostatic repulsion between the Gd^{III}-coordinated –OH group and the protonated basic phosphonate –OH and amino NH^+ moieties of the pendant arm. On the other hand, whereas the protonation constant of the alkoxide $-O^-$ group ($\log K_{GdLH_{-1}}$) of the Gd$\mathbf{L_2}$ complex is comparable to that of Gd(**HP-DO3A**), the $\log K_{GdLH_{-1}}$ value of Gd$\mathbf{L_1}$ is significantly higher. The higher $\log K_{GdLH_{-1}}$ value of the Gd$\mathbf{L_1}$ complex might be explained by the H-bond formation between the remote tertiary amino N donor atom and the coordinated –OH group. The $\log K_{GdLH_{-1}}$ value of the Gd(**HPA-DO3A**) complex that characterizes the protonation of the alkoxide $-O^-$ group is significantly smaller than that of Gd$\mathbf{L_{1,2}}$ and Gd(**HP-DO3A**) due to the presence of the strong electron withdrawing amide group on the hydroxyl-ethyl pendant arm.[16d]

Table 1 Stability and protonation constants of Ca^{II}-, Zn^{II}-, Cu^{II}- and Gd^{III}-complexes formed with $\mathbf{L_1}$, $\mathbf{L_2}$, **HP-DO3A**, **HPA-DO3A** (25 °C)

I	$\mathbf{L_1}$ 0.15 M NaCl	$\mathbf{L_2}$	**HP-DO3A**[a] 0.1 M Me_4NCl	**HPA-DO3A**[b] 0.15 M NaCl
CaL	11.53(3)	11.14(4)	14.83	12.13
ZnL	16.86(4)	16.94(3)	19.37	17.18
[d]CuL	20.99(7)	20.49(1)	22.84	21.53
GdL				
Relax.	19.93(7)	19.16(9)	23.8	18.41
pHpot.	20.25(4)	19.66(8)		
GdHL	7.36 (1)	7.98 (3)	—	—
GdH_2L	4.00 (2)	4.49 (4)	—	—
$GdLH_{-1}$	12.31(1)	11.56(2)	11.31[c]	6.73

[a] Ref. 21. [b] Ref. 16*d*. [c] Ref. 16*b* (0.15 M NaCl, 25 °C). [d] Spectrophotometry.

Kinetic inertness of GdL_1 and GdL_2

The kinetic inertness (kinetic stability) of any metal complexes, *i.e.*: a measure of the propensity for release of free metal ion and ligand, is one of the key parameters for the safe *in vivo* applications. Dissociation of the Ln^{III} complexes formed with tetraazamacrocyclic ligands is extremely slow and generally occurs through the acid-catalyzed decomplexation pathways involving formation of protonated intermediate. Direct attack by the endogenous metal ions is negligible role in the dissociation of these metal complexes.[2a,16d,23] The dissociation reactions of Gd$\mathbf{L_1}$ and Gd$\mathbf{L_2}$ complexes were monitored by ^{1}H-NMR relaxometry (20 MHz and 25 °C) in 0.01–1.0 M HCl solution to establish pseudo-first-order kinetic conditions. The pseudo-first order rate constants (k_d) characterizing the dissociation of the Gd^{III} complexes increase with the increase of $[H^+]$ (Fig. S5†), can be interpreted as the proton assisted dissociation of Gd$\mathbf{L_1}$ and Gd$\mathbf{L_2}$ (k_1) *via* the formation of a protonated intermediate (the protonation presumably occurs on the carboxylate group).[2a,16d,23] The k_d value of the Gd$\mathbf{L_2}$ complex obtained at $[H^+] > 0.16$ M shows that dissociation of the Gd$\mathbf{L_2}$ complex might take place by the attack of a second H^+ ion on the protonated intermediate (k_2). The k_1 and k_2 rate constants characterizing the acid-catalyzed decomplexation paths of the Gd$\mathbf{L_1}$ and Gd$\mathbf{L_2}$ complexes are presented and compared with those of Gd(**HP-DO3A**) and Gd(**HPA-DO3A**) in Table 2, together with the k_d rate constants calculated for pH = 2.0. Using these k_d values the half-lives of dissociation of the complexes ($t_{1/2} = \ln 2/k_d$) were also calculated. Experimental details, as well as the definitions and equations used to obtain the kinetic data, are summarized in ESI.†

Comparison of the k_1 values in Table 2 indicates that the proton-assisted dissociation of the Gd$\mathbf{L_1}$ complex is about 5 times faster than that of Gd$\mathbf{L_2}$. On the other hand, the acid-catalyzed decomplexation rates of Gd$\mathbf{L_2}$ and Gd(**HPA-DO3A**) are very similar and somewhat slower than that of Gd(**HP-DO3A**). The dissociation presumably occurs *via* proton transfer, from the –COOH group to the ring N-atom in the protonated Gd^{III} complexes, resulting in the substitution of the Gd^{III} ion by the H^+ in the coordination cage. It might be assumed that the stronger coordination of the –OH group to the Gd^{III}-ion in Gd$\mathbf{L_2}$ results in less favourable proton transfer to the ring N-atom and slower dissociation of the Gd$\mathbf{L_2}$ complex. Comparison of the dissociation rate (k_d) and half-lives ($t_{1/2} = \ln 2/k_d$,) at pH = 2 confirms the higher kinetic inertness of Gd$\mathbf{L_2}$ compared to Gd$\mathbf{L_1}$ and Gd(**HP-DO3A**) (Table 2).

Table 2 Rate constants (k_i) and half-lives ($t_{1/2}$ = ln 2/k_d) characterising the dissociation reactions of [Gd($L_{1,2}$)], [Gd(**HP-DO3A**)] and [Gd(**HPA-DO3A**)] complexes (0.15 M NaCl, 25 °C)

	Gd$\mathbf{L_1}$	Gd$\mathbf{L_2}$	Gd(**HP-DO3A**)[a]	Gd(**HPA-DO3A**)[b]
$k_1/M^{-1}\ s^{-1}$	$(1.0 \pm 0.1)\times10^{-3}$	$(1.8 \pm 0.1)\times10^{-4}$	2.9×10^{-4}	1.6×10^{-4}
$k_2/M^{-2}\ s^{-1}$	—	$(2.2 \pm 0.2) \times 10^{-4}$	—	—
k_d/s^{-1} pH = 2.0	1.0×10^{-5}	1.8×10^{-6}	2.9×10^{-6}	1.6×10^{-6}
$t_{1/2}$/hour pH = 2.0	18.7	104	66.4	120

[a] Ref. 23*c*. [b] Ref. 16*d*.

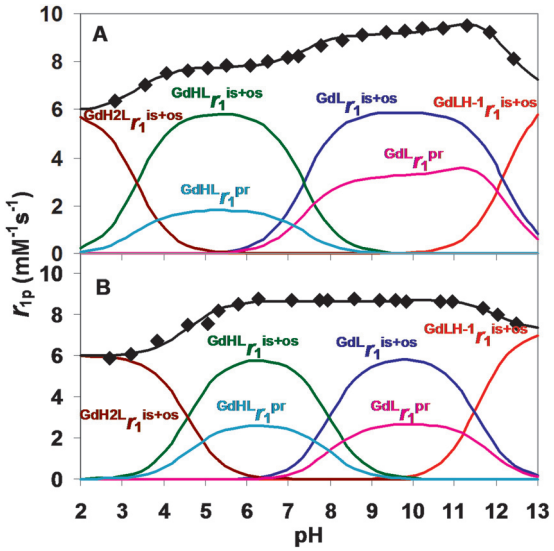

Fig. 1 The relaxivity of Gd$\mathbf{L_1}$ (A) and Gd$\mathbf{L_2}$ (B). Symbols and solid lines represent experimental and calculated relaxivity values, respectively. Calculations have been performed using eqn (3). (20 MHz, 0.15 M NaCl, 298 K).

Relaxation properties of Gd$\mathbf{L_1}$ and Gd$\mathbf{L_2}$ complexes

The effects of the phosphonate group and the amino nitrogen of the pendant arm on the exchange of the –OH proton have been examined by measuring the relaxation enhancement of the Gd$\mathbf{L_1}$ and Gd$\mathbf{L_2}$ complexes as a function of pH (Fig. 1). The relaxivity of Gd(**HP-DO3A**) derivatives is composed of the inner-sphere (r_1^{is}), outer-sphere (r_1^{os}) and the proton exchange (r_1^{pr}) contributions (eqn (1))

$$r_{1p} = r_1^{is} + r_1^{os} + r_1^{pr} \quad (1)$$

The last term in eqn (1) describes the contribution of the proton exchange between the –OH and bulk water protons, which can be expressed by eqn (2).[16]

$$r_1^{pr} = \frac{c}{111.1}\frac{1}{T_{1Pr}^{H} + \tau_{pr}} \quad (2)$$

where, c, T_{1Pr}^{H} and τ_{pr} are the concentration, the longitudinal relaxation time, and the life-time of the –OH proton, respectively.

The relaxivity values of Gd$\mathbf{L_1}$ and Gd$\mathbf{L_2}$ increases in the pH range 3.0–6.0. Since the concentration of the OH^- ion is very low the relaxation enhancement of Gd$\mathbf{L_1}$ and Gd$\mathbf{L_2}$ cannot be explained by the OH^- ion catalyzed proton exchange of the –OH group in this pH range. However, since the deprotonation of the remote basic phosphonate –OH group takes place over the same pH range, the increase in the r_{1p} values might be due to the basis of the deprotonated phosphonate-O^- assisted proton exchange of the –OH group ($^{O}k_{ex}$) in the Gd$\mathbf{L_1}$ and Gd$\mathbf{L_2}$ complexes. In the pH range 6.0–10.0, the relaxivity values of Gd$\mathbf{L_2}$ are constant. However, the relaxivity of Gd$\mathbf{L_1}$ increases from pH = 6.5 to 9.5, then the r_{1p} values remain practically constant with a slightly increase up to pH = 11.5. Since the deprotonation of the tertiary amino-N donor atom takes place in the same pH range, the increase in the r_{1p} values might be due to the simultaneous assistance of the proton exchange of the –OH group by the deprotonated phosphonate-O^- and amino-N donor atoms ($^{N+O}k_{ex}$) in the pendant arm of Gd$\mathbf{L_1}$. The slight increase of the r_{1p} values at pH > 10.0 might be explained by the additional contribution of the OH^- ion catalyzed proton exchange of the –OH group (k_{OH}), which can also contribute to the overall relaxivity of Gd$\mathbf{L_1}$. At higher pH values, the deprotonation of the –OH group causes a decrease in the relaxivity values of the Gd$\mathbf{L_1}$ and Gd$\mathbf{L_2}$ complexes. By taking into account all possible exchange pathways, the exchange life-times of the alcoholic –OH proton is $\tau_{pr} = {}^{O}k_{ex}{}^{-1}$ and $\tau_{pr} = ({}^{N+O}k_{ex} + k_{OH}[OH^-])^{-1}$ for the GdHL and GdL species, respectively. Different r_1^{is} and r_1^{os} contributions to the overall relaxivity of GdH_2L, GdHL, GdL and $GdLH_{-1}$ also to be expected. Considering the total concentration ($[GdL]_t$ = [GdL] + [GdHL] + $[GdH_2L]$ + $[GdLH_{-1}]$ and the protonation constants of the Gd^{III}-complexes ($\log K_{GdHL}$, $\log K_{GdH2L}$, $\log K_{GdLH_{-1}}$, Table 1, eqn (S4) and (S5) in ESI†), eqn (1) can be expressed in the following form:

$$r_{1p} = \frac{1}{1+\alpha_H}\left[{}^{GdH_2L}r_1^{is+os}K_{GdH_2L}K_{GdHL}K_{GdLH_{-1}}[H^+]^3 + {}^{GdHL}r_1^{is+os}K_{GdLH}K_{GdLH_{-1}}[H^+]^2 + {}^{GdL}r_1^{is+os}K_{GdLH_{-1}}[H^+] + {}^{GdLH_{-1}}r_1^{is+os}\right.$$
$$\left. + \frac{K_{GdHL}KGdLH_{-1}[H^+]^2}{111.1}\left(\frac{0.001}{T_{1Pr}^{H} + {}^{O}k_{ex}{}^{-1}}\right) + \frac{K_{GdLH_{-1}}[H^+]}{111.1}\left(\frac{0.001}{T_{1Pr}^{H} + ({}^{N+O}k_{ex} + k_{OH}[OH^-])^{-1}}\right)\right] \quad (3)$$

where $\alpha_H = K_{GdLH_{-1}}[H^+] + K_{GdHL}K_{GdLH_{-1}}[H^+]^2 + K_{GdH2L}K_{GdHL}K_{GdLH_{-1}}[H^+]^3$, ${}^{GdH2L}r_1^{is+os}$, ${}^{GdHL}r_1^{is+os}$, ${}^{GdL}r_1^{is+os}$ and ${}^{GdLH_{-1}}r_1^{is+os}$ are the sum of r_1^{is} and r_1^{os} for GdH_2L, GdHL, GdL and $GdLH_{-1}$ species, respectively. The experimental data (Fig. 1) were fitted to eqn (3) by using a non-linear least squares algorithm and the calculated parameters are listed and compared with those of Gd(**HP-DO3A**) and Gd(**Ph-HP-DO3A**) in Table 3. Since the protonation of the Gd**L$_1$** and Gd**L$_2$** complexes takes place on the remote amino-N and phosphonate–O^- donor atoms of the pendant arms, it was assumed that the sum of r_1^{is} and r_1^{os} of the GdH_2L, GdHL and GdL species are identical for the fitting procedure.

Comparison of the r_1^{is+os} values (Table 3) indicates that the sum of the inner- and outer-contributions of the GdL, GdHL, GdH_2L and $GdLH_{-1}$ species formed by the Gd**L$_1$** and Gd**L$_2$** complex are very similar. However, the r_1^{is+os} values of the GdL, GdHL, GdH_2L and $GdLH_{-1}$ species formed by the Gd**L$_1$** and Gd**L$_2$** complexes are generally about 1.5–2.0 mM^{-1} s^{-1} units higher than those of the corresponding Gd(**HP-DO3A**) and Gd(**HP-DO3A**)H_{-1} complexes, which might be explained by a slower reorientational time of GdL_1 and GdL_2 relative to the parent Gd(**HP-DO3A**) complex. The calculated longitudinal relaxation times of the –OH proton (T_{1Pr}^H, Table 3) of the Gd**L$_1$**, Gd**L$_2$**, Gd(**Ph-HP-DO3A**) and Gd(**HP-DO3A**) complexes are very similar which demonstrates that the relaxation time of the –OH proton in Gd(**HP-DO3A**) derivatives is not influenced by the presence of the different pendant arms. The k_{OH} rate constants of the Gd**L$_1$**, Gd**L$_2$** and Gd(**Ph-HP-DO3A**) are similar and about two orders of magnitude lower than that of Gd(**HP-DO3A**) complex. Based on the general proton transfer theory, the reaction takes place by the continuous formation and breaking of H-bonds between the proton donor and acceptor.[24] Among the influential factors, the formation of the internal H-bond with the exchangeable proton of the donor slows down the general base catalysed intermolecular proton exchange process, due to the hindrance of the H-bond between the proton of the donor and the external acceptor.[24] Considering the protonation constant of the alkoxide –O^- group of Gd**L$_1$** ($\log K_{GdLH_{-1}}$ = 12.31, Table 1), the –OH proton forms a strong H-bond with the deprotonated phosphonate –O^- and amino N donor atoms of the pendant arm, which can inhibit the solution OH^- ion to interact with the –OH proton resulting in the slower OH^- assisted proton exchange of the –OH group. On the other hand, the basic phosphonate-O^- and amino N donor atoms can also catalyse the proton exchange of the –OH group of the Gd**L$_1$** and Gd**L$_2$** complexes. The ${}^Ok_{ex}$ rate constant characterizing the deprotonated phosphonate O^- assisted exchange of the –OH proton of Gd**L$_1$** and Gd**L$_2$** are very similar and comparable with that of basic phenol-O^- assisted proton exchange of the –OH group in Gd(**Ph-HP-DO3A**). However, the rate of the amino N and phosphonate O^- assisted exchange of the –OH proton (${}^{N+O}k_{ex}$) of Gd**L$_1$** is about 1.5 times faster than that of the phosphonate –O^- in the Gd**L$_2$** complex due to the higher basicity of the amino N donor atom ($\log K_{GdHL}$, Table 1). On the other hand, the remote secondary amino N atom does not contribute to the exchange of the –OH proton, which might be explained by the electrostatic repulsion between the –OH and the secondary amino NH groups which overcomes the amino N assisted proton exchange of the –OH group in Gd**L$_2$**.

The relaxivity values of the Gd**L$_1$** and Gd**L$_2$** complexes were also assessed at the imaging fields of 0.47, 1.41 and 3 Tesla and at 37 °C in human plasma (Table 4). In human plasma, the relaxivity values of the Gd**L$_1$** and Gd**L$_2$** complexes decrease by about 3 and 4 mM^{-1} s^{-1} respectively, from 0.47 T to 3 T. Similar phenomena has been identified for Gd(Ph-HP-DO3A) complex.[16c] This finding supports the view that the complexes

Table 4 Relaxivity values (r_{1p}/mM^{-1} s^{-1}) of Gd**L$_1$**, Gd**L$_2$**, Gd(**Ph-HP-DO3A**) (GdPh) and Gd(**HP-DO3A**) (GdHP) complexes at 0.47, 1.41 and 3 T and 310 K in saline (S) and human plasma (HP)

		0.47 T (20 MHz)	1.41 T (60 MHz)	3 T (128 MHz)
Gd**L$_1$**	S	7.1 ± 0.2	6.7 ± 0.1	6.3 ± 0.1
	HP	10.9 ± 0.1	9.5 ± 0.1	7.6 ± 0.1
Gd**L$_2$**	S	8.3 ± 0.3	8.2 ± 0.3	7.5 ± 0.1
	HP	12.5 ± 0.6	10.7 ± 0.5	8.7 ± 0.1
GdPh[a]	S	4.8	4.4	—
	HP	9.1	7.4	—
GdHP[a]	S	3.5	3.0	—
	HP	4.8	4.1	—

[a] Ref. 16c.

Table 3 Kinetic and relaxation parameters for the proton exchange reactions of Gd**L$_1$**, Gd**L$_2$**, Gd(**Ph-HP-DO3A**) and Gd(**HP-DO3A**) complexes (20 MHz, 0.15 M NaCl, 298 K)

	Gd**L$_1$**	Gd**L$_2$**	Gd(**Ph-HP-DO3A**)[a]	Gd(**HP-DO3A**)[b]
${}^{GdH2L}r_1^{is+os}$/mM^{-1} s^{-1}	5.93 ± 0.09	5.99 ± 0.08	—	—
${}^{GdHL}r_1^{is+os}$/mM^{-1} s^{-1}			4.80	—
${}^{GdL}r_1^{is+os}$/mM^{-1} s^{-1}			4.86	4.28
${}^{GdLH-1}r_1^{is+os}$/mM^{-1} s^{-1}	6.7 ± 0.1	6.9 ± 0.1	5.50	4.54
$T_{1Pr}^H \times 10^6$/s	3.0 ± 0.1	3.1 ± 0.3	3.1	5.0
${}^Ok_{ex}$/s^{-1}	(3.4 ± 0.4)×10^5	(7.3 ± 0.7)×10^5	5.6 × 10^5	—
${}^{N+O}k_{ex}$/s^{-1}	(1.0 ± 0.2)×10^6		—	—
k_{OH}/M^{-1} s^{-1}	(8 ± 1)×10^8	(2.5 ± 0.5)×10^8	(8 ± 1)×10^7	1.0 × 10^{10}

[a] Ref. 16a 400 MHz, 298 K, 0.15 M NaCl. [b] Ref. 16d 20 MHz, 298 K, 0.15 M NaCl.

interact with some component(s) present in plasma resulting in systems characterized by a slower reorientational time relative to the parent complexes. As it is well known that aromatic molecules may form host–guest adducts with human serum albumin (HSA)[2] in the case of functionalized Gd^{III}-complexes, the associated elongation of the reorientational correlation time of the paramagnetic system results in marked relaxivity enhancements. The formation of the adduct between $Gd\mathbf{L}_{1,2}$ and HSA was investigated by means of ^1H proton relaxation enhancement (PRE) technique by measuring the variation in the longitudinal relaxation rate (R_1) of the paramagnetic guest for increasing concentrations of the host.[25] In these experiments the R_1 values of the 0.1 mM $Gd\mathbf{L_1}$ and $Gd\mathbf{L_2}$ solutions were measured in the presence of HSA at 20 MHz and 310 K (Fig. S6†). The observed enhancement values presented in Fig. S6† appears consistent simply with the increased viscosity of the albumin solution and therefore the formation of adducts between these complexes and albumin cannot be invoked as the reason for the higher relaxivities shown by the $Gd\mathbf{L_1}$ and $Gd\mathbf{L_2}$ complexes in blood serum.

Moreover, the acquisition of the nuclear magnetic relaxation dispersion (NMRD) profiles of these complexes in serum (Fig. S7†) indicate that the relaxivity humps occur at Larmor frequencies that are a bit lower than the values of 35–40 MHz usually observed for Gd^{III}-complexes interacting with albumin. The position and the entity of the observed relaxation humps are similar to that reported for the related Gd(**Ph-HP-DO3A**) complex, for which an association with the formation of an adduct with albumin was analogously ruled out.[16c] On this basis, we envisage an interaction with slowly moving system(s) that endows the Gd(**HP-DO3A**)-like complexes with motional characteristics slightly different from those commonly expected for the adducts with albumin. The identification of the species responsible for the formation of these supramolecular adducts remains undetermined at the moment. Moreover, we cannot discount the possibility that serum components may contribute to enhance the catalysis of the proton exchange.

X-ray structure of $[Lu\mathbf{L_1}(H_2O)]^{2-}$ complex

To confirm the intramolecular interaction between the –OH group and the remote deprotonated phosphonate-O^- and the amino-N donor atoms of the pendant arm, the crystal structure of the $[Lu\mathbf{L_1}(H_2O)]^{2-}$ complex was determined by X-ray diffraction studies. Specifically, single crystals of formula $\{(C(NH_2)_3)_2[Lu\mathbf{L_1}(H_2O)]\}\cdot 3H_2O$, although of low quality but just suitable for X-ray diffraction studies, were grown by the slow diffusion of an EtOH and Et_2O mixture to aqueous solution of $Lu\mathbf{L_1}$ prepared from equimolar $Lu(OH)_3$ and racemic $H_5\mathbf{L_1}$. To obtain the unprotonated $Lu\mathbf{L_1}$ complex, the pH of the aqueous solution was adjusted to 9 with guanidine-carbonate. A simplified structure of the $[Lu\mathbf{L_1}(H_2O)]^{2-}$ complex with the selected bond distances is presented in Fig. 2. Other details regarding the structure of $[Lu\mathbf{L_1}(H_2O)]^{2-}$ are provided in the ESI.†

The X-ray structure of $[Lu\mathbf{L_1}(H_2O)]^{2-}$ is similar to that of [Gd(**HP-DO3A**)(H_2O)].[26] The asymmetric unit of [Gd(**HP-DO3A**)(H_2O)] contains both capped square antiprismatic (SAP) and

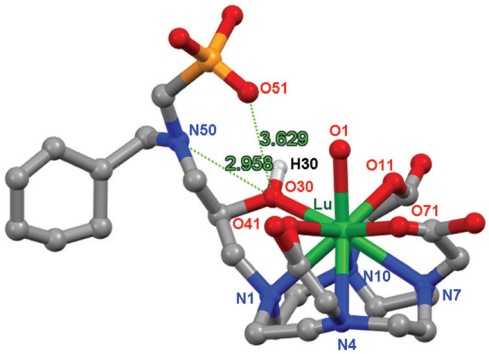

Fig. 2 View of the $[Lu\mathbf{L_1}(H_2O)]^{2-}$ ion present in the single crystal of $\{(C(NH_2)_3)_2[Lu\mathbf{L_1}(H_2O)]\}\cdot 3H_2O$. Hydrogen atoms are omitted for simplicity. Color code: Lu (green), O (red), N (blue) and C (grey). Selected bond distances (Å): Lu–N1 2.65(6), Lu–N4 2.89(6), Lu–N7 2.68(13), Lu–N10 2.94(8), Lu–O1 2.29(4), Lu–O11 2.31(4), Lu–O30 2.37(4), Lu–O41 2.49(5), Lu–O71 2.18(4), O30–O51 3.63(4), O30–N50 2.96(4), O51 – H30 2.96(1) and N50 – H30 3.32(8).

capped twisted square antiprism (TSAP) forms of the Gd(**HP-DO3A**) complex, sharing the same configuration of the chiral 2-hydroxypropyl pendant arm. The crystallization of the racemic [Gd(**HP-DO3A**)(H_2O)] complex occurs with the formation of the conglomerate containing equal amounts of *R* and *S* crystals. In the [Gd(**HP-DO3A**)(H_2O)] complex the Gd^{III}-ion is sandwiched by the two nearly parallel planes formed by nitrogen atoms of the macrocycle and the oxygen atom of the pendant arms. The torsion angle between the two square planes defined by the oxygen and nitrogen atoms are 38° and −28° for the SAP and TSAP stereoisomers of [Gd(**HP-DO3A**)(H_2O)], respectively. The distance of the Gd^{III} ion from the planes formed by the nitrogen and oxygen atoms are 1.61 and 0.75 Å for the SAP and 1.68 and 0.78 Å for TSAP stereoisomers, respectively. The Gd^{III}–OH_2 and Gd^{III}–OH bond distances are 2.51 Å and 2.32 Å for the SAP isomer and 2.50 and 2.35 Å for the TSAP isomer, respectively. The Gd^{III}–N and Gd^{III}–O distances in the [Gd(**HP-DO3A**)(H_2O)] complex are 2.64–2.65 and 2.31–2.38 Å, respectively.

The X-ray diffraction studies of $[Lu\mathbf{L_1}(H_2O)]^{2-}$ reveal that the lattice is centrosymmetric with the triclinic space group of $P\bar{1}$ (No. 2). Three nitrogen, four carboxylate-oxygen, and the alcoholic–oxygen donor atoms of $\mathbf{L_1}$ and one water molecule in the capping position provide the coordination polyhedron around the Lu^{III}-ion in $[Lu\mathbf{L_1}(H_2O)]^{2-}$ (Fig. S9†). Donor atoms of the macrocycle encapsulates the central Lu^{III} ion between the four coplanar nitrogen atoms of the ring (N1, N4, N7 and N10) and the four coplanar oxygen atoms of three acetic and the 2-hydroxypropyl pendant arms (O11, O30, O41 and O71). The ninth apical coordination site of Lu^{III}-ion is occupied by a water molecule (Lu–O1: 2.367 Å) to complete the capped square antiprism geometry (SAP). The distance from the Lu^{III} ion to the O11–O30–O41–O71 and N1–N4–N7–N10 planes is 0.673 and 1.515 Å, respectively. The torsion angle between the two square planes defined by the oxygen and nitrogen atoms is 38°. The bond distances of Lu^{III} with the coordinated N and O donor atoms of $\mathbf{L_1}$ range from 2.65–2.94 Å and 2.18–2.37 Å,

respectively. Importantly, the distances of the –OH proton (H30) from the deprotonated phosphonate–O^- and amino N atoms suggest the formation of a H-bond network which confirms the involvement of these donor atoms in the intramolecular catalysis of the proton exchange of the –OH group with the water protons.

Experimental

Synthesis

A detailed description of all the synthetic procedures and characterizations of intermediates, chelating agents $\mathbf{L_1}$ and $\mathbf{L_2}$ and the corresponding Gd^{III}-complexes can be found in ESI.†

Equilibrium measurements

Materials. The chemicals used for the experiments were of the highest analytical grade. The concentration of the $CaCl_2$, $ZnCl_2$, $CuCl_2$ and $GdCl_3$ solutions were determined by complexometric titration with standardized Na_2H_2EDTA and *xylenol orange* ($ZnCl_2$, and $LnCl_3$), *murexid* ($CuCl_2$) and *Patton & Reeder* ($CaCl_2$) as indicators. The concentration of the $\mathbf{L_1}$ and $\mathbf{L_2}$ ligands was determined by pH-potentiometric titration in the presence and absence of a large (40-fold) excess of $CaCl_2$. The pH-potentiometric titrations were made with standardized 0.2 M NaOH.

Equilibrium measurements. The stability and protonation constants of Ca^{II}, Zn^{II} and Cu^{II} complexes formed with $\mathbf{L_1}$ and $\mathbf{L_2}$ ligand were determined by pH-potentiometric titration. The metal-to-ligand concentration ratio was 1 : 1 with the concentration of the ligand was generally being 0.002 M. The protonation constants of the Gd$\mathbf{L_1}$ and Gd$\mathbf{L_2}$ complexes were determined using pH-potentiometry by titrating the pre-prepared complexes from pH = 3.0 to pH = 12 with 0.2 M NaOH. The stability constants of the Gd$\mathbf{L_1}$ and Gd$\mathbf{L_2}$ complexes were determined by the "out-of-cell" technique because of the slow formation reaction. The pH range of the complexation equilibria and the time needed to reach the equilibria were determined by relaxometry for the formation of Gd$\mathbf{L_1}$ and Gd$\mathbf{L_2}$. Eight Gd^{III}–$\mathbf{L_1}$ and Gd^{III}–$\mathbf{L_2}$ samples were prepared, which had pH values ranging from 2.5–4.0 at equilibrium ($[Gd^{3+}] = [L] = 0.002$ M). The samples were kept at 25 °C for 6 weeks to reach equilibrium. The equilibrium pH and relaxivity values were measured 6 weeks after preparation. The stability constants were calculated both from the measured pH and relaxivity values. For the calculation of the stability constants of the Gd$\mathbf{L_1}$ and Gd$\mathbf{L_2}$ complexes, besides the protonation constants of ligands, the stability constants of the di-protonated *Gd(H_4L) out-of-cage complexes (considered as intermediates) were also used as fixed values. These were calculated from the pH-potentiometric titration curve of the Gd^{3+}–$\mathbf{L_1}$ and Gd^{3+}–$\mathbf{L_2}$ systems obtained in the pH range from 1.7 to 4.0. The relaxivity of the *Gd(H_4L) intermediates were determined by measuring the relaxation rates of 1.0 mM Gd^{3+} and 10 mM $\mathbf{L_1}$ or $\mathbf{L_2}$ ligands (pH = 4.0 with 0.01 M *N*-methyl-piperazine buffer, 0.15 M NaCl, 25 °C) solution as a function of time. The relaxivities of the *Gd(H_4L) intermediates were obtained by extrapolating the measured relaxation rates to the time of mixing of solutions (zero time), when the intermediates were completely formed.

For the pH measurements and titrations, a Metrohm 888 Titrando titration workstation Metrohm-6.0234.110 combined electrode was used. Equilibrium measurements were carried out at a constant ionic strength (0.15 M NaCl) in 6 mL samples at 25 °C. The solutions were stirred, and N_2 was bubbled through them. The titrations were made in the pH range from 1.7 to 12.0. KH-phthalate (pH = 4.005) and borax (pH = 9.177) buffers were used to calibrate the pH meter. For the calculation of $[H^+]$ from the measured pH values, the method proposed by Irving *et al.* was used as follows.[27] A 0.01 M HCl solution was titrated with standardized NaOH solution at 0.15 M NaCl ionic strength. The differences (A) between the measured (pH_{read}) and calculated pH ($-\log[H^+]$) values were used to obtain the equilibrium H^+ concentration from the pH values measured in the titration experiments (A = 0.024). For the equilibrium calculations, the stoichiometric water ionic product (pK_w) was also needed to calculate $[OH^-]$ values under basic conditions. The V_{NaOH}–pH_{read} data pairs of the HCl–NaOH titration obtained in the pH range 10.5–12.0 were used to calculate the pK_w value (pK_w = 13.85).

The stability constants of the Cu$\mathbf{L_1}$ and Cu$\mathbf{L_2}$ complexes were determined by spectrophotometry studying the Cu^{II}–L_1 and Cu^{II}–L_2 systems at the absorption band of Cu^{II} complexes at $[H^+]$ = 0.01–1.0 M in the wavelength range of 400–800 nm. The concentrations of Cu^{II}, $\mathbf{L_1}$ and $\mathbf{L_2}$ were 0.002 M. The H^+ concentration in the samples was adjusted with the addition of calculated amounts of 3 M HCl ($I = [Na^+] + [H^+] = 0.15$, $[H^+] \leq 0.15$ M). The samples were kept at 25 °C for a week. The absorbance values of the samples were determined at 11 wavelengths (575, 595, 615, 635, 655, 675, 695, 715, 735, 755 and 775 nm). To calculate the stability and protonation constants of the Cu$\mathbf{L_1}$ and Cu$\mathbf{L_2}$ complexes, the molar absorptivities of $CuCl_2$, CuL, Cu(HL), Cu(H_2L), Cu(H_3L), Cu(H_4L) and Cu(H_5L) species were determined by recording the spectra of 1.0×10^{-3}, 1.5×10^{-3}, 2.0×10^{-3} and 2.5×10^{-3} M solutions of $CuCl_2$, Cu$\mathbf{L_1}$ and Cu$\mathbf{L_2}$ in the pH range from 1.7 to 12.0. The pH was adjusted by stepwise addition of concentrated NaOH or HCl solutions. The spectrophotometric measurements were made with the use of a PerkinElmer Lambda 365 UV-Vis spectrophotometer at 25 °C, using 1.0 cm cells. The protonation and stability constants were calculated with the PSEQUAD program.[28]

^{1}H and ^{31}P NMR studies. ^{1}H, and ^{31}P NMR measurements were performed either with a Bruker DRX 400 (9.4 T) spectrometer equipped with a Bruker VT-1000 thermocontroller (298 K) and a BB inverse *z* gradient probe (5 mm). The ^{1}H and ^{31}P NMR chemical shifts of $\mathbf{L_1}$ and $\mathbf{L_2}$ were determined as a function of pH to evaluate some of the protonation constants of the ligands. For these experiments, a 0.02 M solution of $\mathbf{L_1}$ and $\mathbf{L_2}$ in 0.15 M NaCl aqueous solution was prepared using a capillary with D_2O for lock. The pH was adjusted by stepwise addition of a solution of NaOH and HCl (both prepared in H_2O). The chemical shifts are reported in ppm, relative to DSS

for ^{1}H and H_3PO_4 for ^{31}P as the external standard. The protonation constants were determined by fitting of the chemical shift *versus* pH data using Micromath Scientist, version 2.0 (Salt Lake City, UT).

^{1}H NMR relaxometry

The relaxivity values (r_1) were calculated from the longitudinal relaxation time of H_2O protons (T_1) measured with a Bruker MQ20 Minispec spectrometer at 20 MHz. The temperature of the sample holder was controlled with a thermostated air stream. The longitudinal relaxation time was measured with the "inversion recovery" method (180°–τ–90°) by using 12 different τ values. The measurements were performed with 1 mM solutions of the **GdL$_1$** and **GdL$_2$** complexes, so the relaxivity values were given as $r_1 = 1/T_{1p} + 1/T_{1w}$ where T_{1p} and T_{1w} were the relaxation time of water protons in the presence and absence of the **GdL$_1$** and **GdL$_2$** complexes. To determine the stability constants of the Gd**L$_1$** and Gd**L$_2$** complexes, we measured the proton relaxation rates of the samples obtained by the "out-of-cell" method in the pH range from 2.5 to 4.0 ([Gd^{III}] = [**L$_{1,2}$**] = 0.002 M, 25 °C, 0.15 M NaCl). In the equilibrium systems besides the free Gd^{III}-ions and Gd(H$_2$**L$_{1,2}$**) complexes, some *Gd(H$_4$**L$_{1,2}$**) out-of-cage complexes (intermediate) were also present. Although it had low concentration (<10%), its contribution to the relaxivity was substantial because of about 4 or 5 coordinated water molecules in the inner-sphere of the Gd^{III} ion. The relaxivity of the four-protonated *Gd(H$_4$**L$_{1,2}$**) out-of-cage complex was calculated from the relaxivity – time kinetic curve obtained for the reaction of 1 mM Gd^{3+} with 10 mM of **L$_{1,2}$** at pH = 4.0, 20 MHz and 25 °C. The variable pH relaxivity measurements of the Gd**L$_{1,2}$** complexes could be carried out by direct titration of the samples at higher pH values (4.5 < pH < 12.5; [Gd**L$_{1,2}$**] = 1.0 mM, 20 MHz and 25 °C, 0.15 M NaCl).

The r_1 values of the **GdL$_1$** and **GdL$_2$** complexes at 37 °C and 0.47 T (20 MHz), 1.41 T (60 MHz) and 3 T (125 MHz) were measured with Bruker Minispec MQ-20 and MQ-60 relaxometers and with a Bruker Biospec 30/40 MRI spectrometer at pH = 7.4 in 0.15 M NaCl solution and in human plasma (control Plasma N, *Siemens*). To study the interaction with HSA, the r_1 values of the **GdL$_1$** and **GdL$_2$** complexes were measured with a Bruker Minispec MQ-20 relaxometer at pH = 7.4, 20 MHz and 37 °C in the presence of 0, 0.1, 0.2, 0.4, 0.6, 0.8, 1, and 2 mM HSA ([GdL] = 0.1 mM).

NMRD profiles were recorded on a Stelar SpinMaster Fast-Field-Cycling (FFC) relaxometer at a continuum of proton frequencies from 0.01 MHz to 20 MHz; additional points were obtained between 21.5 MHz and 70 MHz with a Bruker WP80 electromagnet coupled to a Stelar SpinMaster spectrometer. Both systems were equipped with Stelar VTC-91 temperature control and the internal temperature checked with a calibrated RS PRO RS55-11 digital thermometer. Measures were carried out at 37 °C. The two samples consisted of 1 mM Gd**L$_1$** or Gd**L$_2$** complexes in human plasma. Data, reported as r_{1p}, were obtained by subtracting the diamagnetic contribution of pure plasma from the observed relaxation rates as a function of the magnetic field strength.

Kinetic studies

The kinetic inertness of the Gd**L$_1$** and Gd**L$_2$** complexes was characterized by the rates of the dissociation reactions taking place in 0.01–1.0 M HCl solution. The dissociation reactions of the Gd^{III}-complex were followed by measuring the longitudinal relaxation time of H_2O protons (T_1) with a Bruker MQ20 Minispec spectrometer at 20 MHz. The temperature of the sample holder was controlled with a thermostated air stream. The longitudinal relaxation time was measured with the "inversion recovery" method (180°–τ–90°) by using 12 different τ values. The measurements were performed with 1 mM solution of Gd**L$_1$** and Gd**L$_2$** complex. The relaxivity values were given as $r_1 = 1/T_{1p} + 1/T_{1w}$ where T_{1p} and T_{1w} are the relaxation times of the bulk water protons in the presence and absence of Gd^{III}-complex. The pseudo-first-order rate constants (k_d) were calculated by fitting the relaxation rate ($r_1 = 1/T_{1p}$) data to eqn (4).

$$r_t = (r_r - r_v)e^{(-k_d t)} + r_v \quad (4)$$

where r_r, and r_v are the relaxivity values of the reactants, the product (Gd^{III}: r_{1p} = 13.12 (2) mM^{-1} s^{-1}, 20 MHz, 25 °C) and r_t is the measured relaxivity at reaction time t. The temperature was maintained at 25 °C and the ionic strength of the solutions was kept constant at [H$^+$] ≤ 0.15 M, [HCl] + [NaCl] = 0.15 M. The calculation of the kinetic parameters were performed by the fitting of the absorbance – time and relaxation rate – time data pairs with the Micromath Scientist computer program (version 2.0, Salt Lake City, UT, USA).

X-ray diffraction studies

Single crystals of {(C(NH$_2$)$_3$)$_2$[Lu**L$_1$**(H$_2$O)]}·3H$_2$O were obtained by the slow diffusion of EtOH and Et$_2$O mixture to aqueous solution of Lu**L$_1$** prepared by equimolar Lu(OH)$_3$ and racemic H$_5$**L$_1$**. The pH of the Lu**L$_1$** solution was adjusted to 9 with guanidine-carbonate. Several crystals were studied and XRD data collection was carried out at 293 K using Mo-Kα radiation (λ = 0.71073 Å) with a Burker-Nonius MACH3 diffractometer equipped with point detector. Unexpectedly, all crystals diffracted rather weakly, even the large volume ones and the peaks were very diffuse, an example is shown in Fig. S8.† Moreover, crystals were decomposing under X-ray radiation, showing a decay of 40%. Even low temperature data collection could not give better results as crystals further degraded by cooling and in spite of several attempts no further batches of crystals could be prepared. After careful integration the structure could be solved by SIR-92 program[29] and refined by full-matrix least-squares method on F^2 using the SHELX program.[30] Unfortunately, only heavy Lu^{III}-ion and phosphorous atoms could be refined with anisotropic atomic displacement parameters using the SHELX package while the light atoms needed to be kept isotropic to prevent collapse of the refinement. Fortunately the atoms and their connectivity to the ligand could be localized, in some cases even hydrogen atoms of the solvent water molecules could be found on the difference electron density map. Remaining significant peaks were very close to the Lu^{III} ion. Distances of hydrogen and oxygen atoms were

restrained in the final stage of the refinement and several other enhanced rigid-bond restraints (RIGU) were applied to regulate thermal parameters of carbon atoms. Altogether hydrogen atoms were treated with a mixture of independent and constrained refinement. Publication material was prepared with the WINGX-suite.[31] Also, especially the water molecules had significant shifts even after prolonged refinement. These features of the structure resulted in high *R* values, shift, and several 'A' and 'B' level errors in the checkcif report. Nevertheless the overall structure of the complex is sufficient to answer the structural questions *i.e.* coordination of Lu^{III} and indicate extensive and complex hydrogen bond network, for a simplified packing diagram see Fig. S10.† Further crystallographic data are shown in the ESI and deposited in the Cambridge Crystallographic Data Centre under CCDC 2042633.†

Conclusions

Our results show that the relaxivity of Gd-**HPDO3A** can be markedly increased at physiological pHs by exploiting the prototropic exchange of the coordinated hydroxy group when a proper intramolecular H-bonding framework is set up. A phosphonic moiety appears to be particularly useful as the deprotonated phosphate oxygen may act as proton acceptor (from the coordinated alcoholic group). It may be the site for operating a fast prototropic exchange with the bulk water solvent. Also, the N-sites, both in $\mathbf{L_1}$ and $\mathbf{L_2}$, appear to play a role in establishing the H-bonding network. Importantly, the chemical modifications performed on the **HP-DO3A** ligand, leading to the improved prototropic exchange of these new Gd^{III} complexes, do not compromise their thermodynamic and kinetic properties. These observations, together with the fact that phosphonates may not be used "*in vivo*" since they are bone-seekers, may likely lead to the design of related systems by changing the characteristics of the proton accepting/donating groups in the set-up of the H-bonding with the coordinated –OH functionality. Moreover, the aromatic substituent on the surface of the complex appears instrumental to promote an interaction with serum components that, in turn, results in a further enhancement of the relaxivity in this medium.

Conflicts of interest

LL, SCS, AFM and ZB are employees of Bracco Group, the manufacturer of gadoteridol.

Acknowledgements

A. B. thanks the Hungarian National Research, Development and Innovation Office – NKFIH under the Grant NKFI NN 128368. D. H.: University of Debrecen, Faculty of Science and Technology, Department of Physical Chemistry, Doctoral School of Chemistry.

References

1 (*a*) D. B. Plewes and W. Kucharczyk, Physics of MRI: A Primer, *J. Magn. Reson. Imaging*, 2012, **35**, 1038–1054; (*b*) M. Bottrill, L. Kwok and N. J. Long, Lanthanides in magnetic resonance imaging, *Chem. Soc. Rev.*, 2006, **35**, 557–571.

2 (*a*) *The Chemistry of Contrast Agents in Medical Magnetic Resonance Imaging*, ed. A. Merbach, L. Helm and É. Tóth, Wiley, New York, 2nd edn, 2013; (*b*) R. B. Lauffer, Paramagnetic Metal Complexes as Water Proton Relaxation Agents for NMR Imaging: Theory and Design, *Chem. Rev.*, 1987, **87**, 901–927.

3 (*a*) V. M. Runge, T. Ai, D. Hao and X. Hu, The Developmental History of the Gadolinium Chelates as Intravenous Contrast Media for Magnetic Resonance, *Invest. Radiol.*, 2011, **46**, 807–816; (*b*) C. F. G. C. Geraldes and S. Laurent, Classification and basic properties of contrast agents for magnetic resonance imaging, *Contrast Media Mol. Imaging*, 2009, **4**, 1–23; (*c*) P. Hermann, J. Kotek, V. Kubíček and I. Lukeš, Gadolinium(III) complexes as MRI contrast agents: ligand design and properties of the complexes, *Dalton Trans.*, 2008, 3027–3047; (*d*) P. Caravan, J. J. Ellison and T. J. McMurry, Gadolinium(III) Chelates as MRI Contrast Agents: Structure, Dynamics, and Applications, R. B. Lauffer, *Chem. Rev.*, 1999, **99**, 2293–2352.

4 (*a*) A. D. Sherry, P. Caravan and R. E. Lenkinski, Primer on Gadolinium Chemistry, *J. Magn. Reson. Imaging*, 2009, **30**, 1240–1248; (*b*) T. J. Clough, L. Jiang, K.-L. Wong and N. J. Long, Ligand design strategies to increase stability of gadolinium-based magnetic resonance imaging contrast agents, *Nat. Commun.*, 2019, **10**, 1420.

5 S. Laurent, C. Henomount, L. Vander Elst and R. N. Muller, Synthesis and Physicochemical Characterisation of Gd-DTPA Derivatives as Contrast Agents for MRI, *Eur. J. Inorg. Chem.*, 2012, 1889–1915.

6 G. J. Stasiuk and N. J. Long, The ubiquitous DOTA and its derivatives: the impact of 1,4,7,10-tetraazacyclododecane-1,4,7,10-tetraacetic acid on biomedical imaging, *Chem. Commun.*, 2013, **49**, 2732–2746.

7 Y. Shen, F. L. Goerner, C. Snyder, J. N. Morelli, D. Hao, D. Hu, X. Li and M. Val Runge, T1 Relaxivities of Gadolinium-Based Magnetic Resonance Contrast Agents in Human Whole Blood at 1.5, 3, and 7 T, *Invest. Radiol.*, 2015, **50**, 330–338.

8 (*a*) S. B. Cho, A.-L. Lee, H. W. Chang, K. A. Kim, W. J. Yoo, J. A. Yeom, M. H. Rho, S. J. Kim, Y.-J. Lim and M. Han, Prospective Multicenter Study of the Safety of Gadoteridol in 6163 Patients, *J. Magn. Reson. Imaging*, 2020, **51**, 861–868; (*b*) E. Kanal and M. F. Tweedle, Residual or Retained Gadolinium: Practical Implications for Radiologists and Our Patients, *Radiology*, 2015, **275**, 630–634; (*c*) J. M. Hazelton, M. K. Chiu and H. H. Abujudeh, Nephrogenic Systemic Fibrosis: A Review of History, Pathophysiology, and Current Guidelines, *Curr. Radiol. Rep.*, 2019, **7**, 5.

9 (*a*) E. Gianolio, E. Di Gregorio and S. Aime, Chemical Insights into the Issues of Gd Retention in the Brain and Other Tissues Upon the Administration of Gd-Containing MRI Contrast Agents, *Eur. J. Inorg. Chem.*, 2019, 137–151; (*b*) M. Le Fur and P. Caravan, The biological fate of gadolinium-based MRI contrast agents: a call to action for bioinorganic chemists, *Metallomics*, 2019, **11**, 240–254; (*c*) A. Stanescu, D. Shaw, N. Murata, K. Murata, J. Rutledge, E. Maloney and K. Maravilla, Brain tissue gadolinium retention in pediatric patients after contrast-enhanced magnetic resonance exams: pathological confirmation, *Pediatr. Radiol.*, 2020, **50**, 388–396.

10 C. Robic, M. Port, O. Rousseaux, S. Louguet, N. Fretellier, S. Catoen, C. Factor, S. Le Greneur, C. Medina, P. Bourrinet, I. Raynal, J.-M. Idée and C. Corot, Physicochemical and Pharmacokinetic Profiles of Gadopiclenol. A New Macrocyclic Gadolinium Chelate With High T1 Relaxivity, *Invest. Radiol.*, 2019, **54**, 475–484.

11 S. Aime, M. Botta, S. Geninatti Crich, G. B. Giovenzana, G. Jommi, R. Pagliarin and M. Sisti, Synthesis and NMR Studies of Three Pyridine-Containing Triaza Macrocyclic Triacetate Ligands and Their Complexes with Lanthanide Ions, *Inorg. Chem.*, 1997, **36**, 2992–3000.

12 (*a*) M. F. Tweedle, New Developments in Magnetic Resonance Contrast Media. A Global Perspective on Gadoteridol—Introduction, *Invest. Radiol.*, 1992, **27**, S2–S6; (*b*) V. M. Runge, Clinical Safety of Gadoteridol, Representative of the Macrocyclic Class of Gadolinium–Based Contrast Agents, *J. Magn. Reson. Imaging*, 2020, **51**, 869–870.

13 (*a*) S. Aime, M. Chiaussa, G. Digilio, E. Gianolio and E. Terreno, Contrast agents for magnetic resonance angiographic applications: ^{1}H and ^{17}O NMR relaxometric investigations on two gadolinium(III) DTPA-like chelates endowed with high binding affinity to human serum albumin, *J. Biol. Inorg. Chem.*, 1999, **4**, 766–774; (*b*) S. Aime, M. Botta, M. Fasano, S. Geninatti Crich and E. Terreno, Gd(III) complexes as contrast agents for magnetic resonance imaging: a proton relaxation enhancement study of the interaction with human serum albumin, *J. Biol. Inorg. Chem.*, 1996, **1**, 312–319.

14 F. M. Cavagna, F. Maggioni, P. M. Castelli, M. Daprà, L. G. Imperatori, V. Lorusso and B. G. Jenkins, Gadolinium Chelates with Weak Binding to Serum Proteins: A New Class of High-Efficiency, General Purpose Contrast Agents for Magnetic Resonance Imaging, *Invest. Radiol.*, 1997, **32**, 780–796.

15 F. L. Giesel, H. von Tengg-Kobligk, I. D. Wilkinson, P. Siegler, C.-W. von der Lieth, M. Frank, K. P. Lodemann and M. Essig, Influence of human serum albumin on longitudinal and transverse relaxation rates (R_1 and R_2) of magnetic resonance contrast agents, *Invest. Radiol.*, 2006, **41**, 222–228.

16 (*a*) I. M. Carnovale, M. L. Lolli, S. Colombo Serra, A. Fringuello Mingo, R. Napolitano, V. Boi, N. Guidolin, L. Lattuada, F. Tedoldi, Z. Baranyai and S. Aime, Exploring the intramolecular catalysis of the proton exchange process tomodulate the relaxivity of Gd(III)-complexes of HP-DO3A-like ligands, *Chem. Commun.*, 2018, **54**, 10056–10059; (*b*) S. Aime, S. Baroni, D. Delli Castelli, E. Brücher, I. Fábián, S. Colombo Serra, A. Fringuello Mingo, R. Napolitano, L. Lattuada, F. Tedoldi and Z. Baranyai, Exploiting the Proton Exchange as an Additional Route to Enhance the Relaxivity of Paramagnetic MRI Contrast Agents, *Inorg. Chem.*, 2018, **57**, 5567–5574; (*c*) A. Fringuello Mingo, S. Colombo Serra, S. Baroni, C. Cabella, R. Napolitano, I. Hawala, I. M. Carnovale, L. Lattuada, F. Tedoldi and S. Aime, Macrocyclic Paramagnetic Agents for MRI: Determinants of Relaxivity and Strategies for Their Improvement, *Magn. Reson. Med.*, 2017, **78**, 1523–1532; (*d*) L. Leone, M. Boccalon, G. Ferrauto, I. Fábián, Zs. Baranyai and L. Tei, Acid-catalyzed proton exchange as a novel approach for relaxivity enhancement in Gd-HPDO3A-like complexes, *Chem. Sci.*, 2020, **11**, 7829–7835.

17 (*a*) L. Lattuada, A. Barge, G. Cravotto, G. B. Giovenzana and L. Tei, The synthesis and application of polyamino polycarboxylic bifunctional chelating agents, *Chem. Soc. Rev.*, 2011, **40**, 3019–3049; (*b*) L. Frullano and P. Caravan, Strategies for the Preparation of Bifunctional Gadolinium (III) Chelators, *Curr. Org. Synth.*, 2011, **8**, 535–565; (*c*) G. B. Giovenzana, L. Lattuada and R. Negri, Recent Advances in Bifunctional Paramagnetic Chelates for MRI, *Isr. J. Chem.*, 2017, **57**, 825–832.

18 L. Lattuada, R. Napolitano, V. Boi, M. Visigalli, S. Aime, G. B. Giovenzana and A. Fringuello Mingo, Contrast Agents, *Int. Pat. Appl* WO2017/09838, 2017.

19 H. C. Manning, M. Bai, B. M. Anderson, R. Lisiak, L. E. Samuelson and D. J. Bornhop, Expeditious synthesis of 'P'-protected macrocycles en route to lanthanide chelate metal complexes, *Tetrahedron Lett.*, 2005, **46**, 4707–4710.

20 J. Wahsner, E. M. Gale, A. Rodríguez-Rodríguez and P. Caravan, Chemistry of MRI Contrast Agents: Current Challenges and New Frontiers, *Chem. Rev.*, 2019, **119**, 957–1057.

21 K. Kumar, M. F. Tweedle, M. F. Malley and J. Z. Gougoutas, Synthesis, Stability, and Crystal Structure Studies of Some Ca^{2+}, Cu^{2+}, and Zn^{2+} Complexes of Macrocyclic Polyamino Carboxylates, *Inorg. Chem.*, 1995, **34**, 6472–6480.

22 R. Delgado and J. J. R. Fraústo Da Silva, Metal complexes of cyclic tetra-azatetra-acetic acids, *Talanta*, 1982, **29**, 815–822.

23 (*a*) K. Kumar, T. Jin, X. Wang, F. Desreux and M. F. Tweedle, Effect of Ligand Basicity on the Formation and Dissociation Equilibria and Kinetics of Gd^{3+} Complexes of Macrocyclic Polyamino Carboxylates, *Inorg. Chem.*, 1994, **33**, 3823–3829; (*b*) É. Tóth, E. Brücher, I. Lázár and I. Tóth, Kinetics of Formation and Dissociation of Lanthanide(III)-DOTA Complexes, *Inorg. Chem.*, 1994, **33**, 4070–4076; (*c*) Z. Baranyai, Z. Pálinkás, F. Uggeri, A. Maiocchi, S. Aime and E. Brücher, Dissociation Kinetics of Open–Chain and Macrocyclic Gadolinium(III)–Aminopolycarboxylate Complexes Related to Magnetic Resonance Imaging: Catalytic Effect of

Endogenous Ligands, *Chem. – Eur. J.*, 2012, **18**, 16426–16435; (*d*) L. Tei, Zs. Baranyai, L. Gaino, A. Forgács, A. Vágner and M. Botta, Thermodynamic stability, kinetic inertness and relaxometric properties of monoamide derivatives of lanthanide(III) DOTA complexes, *Dalton Trans.*, 2015, 5467–5478.

24 M. Eigen, Proton Transfer, Acid–Base Catalysis, and Enzymatic Hydrolysis. Part I: ELEMENTARY PROCESSES, *Angew. Chem., Int. Ed. Engl.*, 1964, **3**, 1–19.

25 R. A. Dwek, *Nuclear Magnetic Resonance (N.M.R.) in Biochemistry*, Oxford University Press, Oxford, 1973.

26 K. Kumar, C. A. Chang, L. C. Francesconi, D. D. Dischino, M. F. Malley, J. Z. Gougoutas and M. F. Tweedle, Synthesis, Stability, and Structure of Gadolinium(III) and Yttrium(III) Macrocyclic Poly(amino carboxylates), *Inorg. Chem.*, 1994, **33**, 3567–3575.

27 H. M. Irving, M. G. Miles and L. D. Pettit, A study of some problems in determining the stoicheiometric proton dissociation constants of complexes by potentiometric titrations using a glass electrode, *Anal. Chim. Acta*, 1967, **38**, 475–488.

28 L. Zekany, I. Nagypal and I. In, *Computational Methods for the Determination of Formation Constants*, ed. D. Leggett, Springer US, 1985, p. 291.

29 A. Altomare, G. Cascarano, C. Giacovazzo, A. Guagliardi, M. C. Burla, G. Polidori and M. Camalli, SIR92 – a program for automatic solution of crystal structures by direct methods, *J. Appl. Crystallogr.*, 1994, **27**, 435.

30 G. M. Sheldrick, SHELXL, version 2016/4; Crystal structure refinement with SHELXL, *Acta Crystallogr., Sect. C: Struct. Chem.*, 2015, **71**, 3–8.

31 L. J. Farrugia, WinGX and ORTEP for Windows: an update, *J. Appl. Crystallogr.*, 2012, **45**, 849–854.